Three-Dimensional Structure and Dynamics of Wine Tannin−Saliva Protein Complexes. A Multitechnique Approach†

Cécile Simon,‡ Karine Barathieu,§ Michel Laguerre,‡ Jean-Marie Schmitter,‡ Eric Fouquet,§ Isabelle Pianet,*,‡,§ and Erick J. Dufourc‡

Institut Européen de Chimie et Biologie, UMR CNRS 5144, Pessac, France, and Laboratoire de Chimie Organique et Organométallique, UMR CNRS 5802, Talence, France

Received March 5, 2003; Revised Manuscript Received June 13, 2003

ABSTRACT: The interactions between the B3 (catechin-4α,8-catechin) red wine tannin and the human salivary protein fragment $IB7_{14}$ (SPPGKPQGPPPQGG) were monitored by ^1H magic angle spinning NMR, circular dichroism, electrospray ionization mass spectrometry, and molecular modeling. It is found that the secondary structure of $IB7_{14}$ is made of a type II helix (collagen helix) and random coil. The central glycine 8 appears to act as a flexible rotula separating two helix II regions. Three tannin molecules tightly complex the peptide, without modifying its secondary structure, but seem to reduce its conformational dynamics. The binding dissociation constant is in the millimolar range. B3 tannins with a "tweezers" conformation bind to the hydrophilic side of the saliva peptide, suggesting that the principal driving forces toward association are governed by hydrogen bonding between the carbonyl functions of proline residues and both the phenol and catechol OH groups. These findings are further discussed in the frame of an astringency phenomenon.

Astringency is an important mouth-feel character determining the quality of red wine. This sensation, earlier considered by Aristotle (384−322 B.C.) as a taste, was described in physicochemical terms by Joslyn and Golstein in 1964 (*1*) as the result of a strong interaction between tannins and salivary proteins. The formed tannin−protein complex aggregates, thus reducing the lubricating property of saliva (*2*, *3*). A dry, rough, and pucker sensation is then perceived as a diffuse stimulus in the entire mouth (*4*−*6*).

Tannins responsible for wine astringency are mostly flavan-3-ol polymers commonly referred to as proanthocyanidins or condensed tannins (*7*); they are extracted from grape skins and seeds during the maceration phase of wine-making and may reach a concentration up to 4 g/L in Bordeaux red wine (*8*).

About 70% of the human salivary proteins secreted by the parotid gland are proline-rich proteins (PRPs)[1] (*9*, *10*). They are made up of three types: acidic, glycosylated, and basic (*11*). The specific role of each type is not clear yet, but recent studies suggest multiple protective functions such as virus binding (*12*). Acidic PRPs could maintain calcium homeostasis (*9*, *13*), while glycosylated ones could play a role in the oral cavity lubrication (*14*) and prevent bacterial agglutination (*15*). Nevertheless, the only known biological function of basic PRPs is to bind polyphenols (*16*−*18*). All of these PRPs share a high degree of homology, because they are encoded by a small number of genes (*19*). Their unique composition, where proline, glycine, and glutamine account for 70−80% of the total amino acid content (*20*), confers to PRPs an extended and opened structure (*21*) that may be favorable to tannin binding. Also they are made in repeated patterns of five aa (PQGPP) and nine aa (PPGKPQGPP). Among them, the IB7 protein appears to be a generic protein whose sequence is almost entirely found in many other PRPs.

Interactions occurring between tannins and proteins were largely studied this past decade. An understanding of this phenomenon is of great interest in order to characterize the gustative sensation called astringency in foods and beverages (*22*). It is also of interest to control the production of leather or to define the role of tannins in medicine, a fashionable theme after the "French paradox" hypothesis (*23*). The above studies were carried out by using models such as the proline amino acid alone, the tetrapeptide Gly-Pro-Gly-Gly (*24*), the nonapeptide bradykinin (*25*−*27*), angiotensins I and II (*27*), PRP typical repeat units (*28*−*30*), and even an entire PRP (*31*−*33*). For the tannin counterpart, catechin, epicatechin, procyanidin B3, or hydrolyzable tannins such as tri-, tetra- and pentagalloylglucose were used. Various experiments were used in these contributions to highlight protein−tannin interactions, including solution NMR, molecular modeling,

† This work is supported by grants from the Conseil Interprofessionnel du Vin de Bordeaux (CIVB).

* Address correspondence to this author. Tel: +33556846448. Fax: +33556842623. E-mail: i.pianet@cesamo.u-bordeaux.fr.

‡ Institut Européen de Chimie et Biologie.

§ Laboratoire de Chimie Organique et Organométallique.

[1] Abbreviations: aa, amino acids; CD, circular dichroism; CID, collision-induced dissociation; DQF-COSY, double-quantum filtered correlation spectroscopy; DIPSI, decoupling in the presence of scalar interactions; ESI, electrospray ionization; HOHAHA, homonuclear Hartmann−Hahn; HRMAS, high-resolution magic angle spinning; MALDI, matrix-assisted laser desorption ionization; MS, mass spectrometry; *m*/*z*, mass over charge ratio; NMR, nuclear magnetic resonance; PRPs, proline-rich proteins of saliva; RMSD, root mean square deviation; ROESY, rotating frame enhancement spectroscopy; Th, Thomson (unit for *m*/*z* ratio); WATERGATE, WATER suppression by gradient-tailored excitation.

10.1021/bi034354p CCC: $25.00
Published on Web 08/13/2003

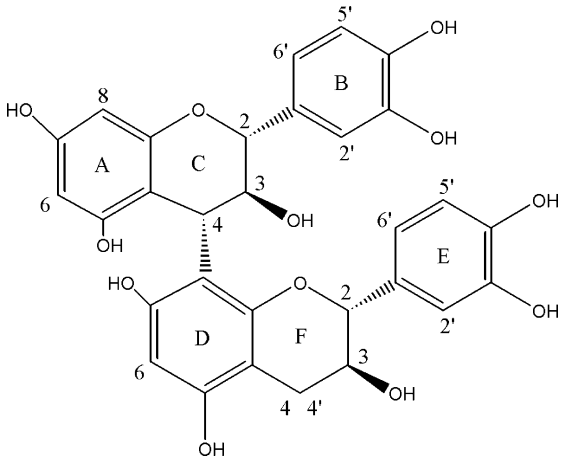

FIGURE 1: Schematic representation of the B3 procyanidin dimer, catechin-4α,8-catechin.

mass spectrometry, and gel electrophoresis. Hydrophobic effects have been considered in various papers as the main driving forces toward association (*26*, *27*), probably enhanced by hydrogen bonding between the phenolic groups and the protein, mainly through the carbonyl groups of prolines (*34*). Nonetheless, it is commonly thought that a specific mode of binding between polyphenols and a PRP is highly improbable. The nature of the interaction probably depends on the nature of the polyphenol, its size, its stereochemistry, the nature of the protein, and the medium in which the interaction takes place. Moreover, one of the difficulties encountered in these studies is the formation of a colloidal insoluble complex in water, requiring to work in a solvent mixture containing DMSO (10−20%), that is far from representing the wine and mouth medium.

In the present work, we describe the interactions of the B3 procyanidin (catechin-4α,8-catechin) (Figure 1) with a 14-residue fragment of IB7. Unlike others, we decided to study the association in a medium as close as possible to reality, i.e., water−ethanol (88:12 v/v), pH 3.5. Noninvasive methods such as solid-state NMR by HRMAS, mass spectrometry in MALDI and electrospray modes, circular dichroism, and molecular mechanics have been used to determine the 3D structure, the stoichiometry in the complex, the dissociation constant, and the dynamics of the aggregates.

MATERIALS AND METHODS

Chemicals. Amino acids, solid-phase support, HOBt, and HBTU for solid-phase synthesis were purchased from Novabiochem (Läufelfingen, Switzerland). Catechin was obtained from Sigma (Sigma-Chimie, France), and other solvents for synthesis and HPLC were from SDS (Peypin, France).

Peptide Synthesis and Purification. The chemical synthesis of the IB7 peptide ($IB7_{14}$: SPPGKPQGPPPQGG) was performed on an Applied Biosystems peptide synthesizer 433A (PE Biosystem, Courtaboeuf, France) by the FastMoc method on a solid state, using the method that we have described previously (*21*). After purification by reversed-phase liquid chromatography over a C18 column (Alliance chromatographic system, Waters, Saint-Quentin-en-Yvelynes, France), the product was analyzed by MALDI mass spectrometry.

B3 Synthesis. The synthesis of the catechin-4α,8-catechin dimer, procyanidin B3 (Figure 1), was achieved with the method described by Tückmantel et al. (*35*), with slight modifications (*36*, *37*).

Circular Dichroism. Far-ultraviolet (190−370 nm) circular dichroism spectra were recorded on a Mark VI Jobin-Yvon dichrograph (Longjumeau, France), calibrated with isoandrosterone (Roussel-Uclaf, France) in dioxane and camphorsulfonic acid (Sigma-Chimie, France) as previously described (*38*). Measurements were carried out at room temperature with 1 or 0.1 mm path length cells, in water or in a water−ethanol mixture (88:12 v/v), pH 3.5, obtained by dropwise addition of HCl. Titrations were performed as follows: Procyanidin B3 solution (0.025−1 mM final concentration) was progressively added to a 0.1 mM peptide sample, or, at the opposite, the B3 concentration was fixed to 0.1 mM and the peptide concentration was varied from 0.025 mM to 1 mM. Both procedures gave the same result.

Mass Spectrometry. Mass analysis of the $IB7_{14}$ peptide was performed on a MALDI mass spectrometer in the reflectron mode (Bruker Reflex III) using α-cyano-4-hydroxycinnamic acid as a matrix.

An ion trap mass spectrometer equipped with a nanospray interface (LCQ Deca XP, Thermo Finnigan) was used for peptide−tannin interaction studies. Premixed peptide tannin solutions in water−ethanol−acetic acid (89:10:1 v/v/v), pH 3.5, were infused with needles having 2 μm orifices (New Objective) at a 10 μM $IB7_{14}$ peptide concentration. The temperature of the heated capillary in the interface was set to 150 °C, and the spraying voltage was 1.2 kV. Doubly charged species corresponding to peptide−tannin complexes were isolated in the ion trap with a ±3 Da isolation width and disrupted using a collision energy of 18−23% on the instrument's scale.

NMR Spectroscopy. The samples were prepared as follows: the lyophilized synthetic peptide was dissolved in a H_2O-D_2O mixture (90:10) with or without 12% deuterated ethanol to 1−5 mM concentration. When needed, procyanidin B3 was added in order to obtain the desired concentrations (between 0 and 13 mM). The pH of the solution mixtures was then adjusted to 3.5. Eighty microliters of each sample was then poured into a 4 mm HRMAS rotor. The 1D and 2D NMR spectra were recorded on a Bruker Avance DSX 500 spectrometer using a dual HRMAS probe with ^2H lock and equipped with a *z**-gradient. Spectra were recorded with a spinning rate of 5000 Hz at 300 K. The water resonance was suppressed using the watergate sequence (*39*). The 1D proton spectra were recorded for titration using standard conditions (single pulse sequence, 256 scans, recycling delay 3 s). DQF-COSY, HOHAHA, and ROESY spectra were acquired in the phase-sensitive mode with time-proportional phase incrementation (TPPI) of the first pulse (*40*). The proton 90° pulse was 5.9 μs, and the spectral width was set to 10 ppm (5000 Hz) in both dimensions. HOHAHA spectra were recorded using the MLEV pulse scheme with 100 and 150 ms isotropic mixing periods. ROESY spectra were recorded with a 300 ms spin-lock time (0.3 W, 1.5 kHz). The data size was usually 2048 complex points in the t_2 dimension, and 512 t_1 increments were performed. A total of 128 scans were acquired for the HOHAHA spectrum and 256 scans for COSY and ROESY experiments. GIFA software was used to process the NMR data (*41*, *42*). After

zero filling to 2K in both dimensions, the two-dimensional data matrices were multiplied by a shifted sine-bell window function (sin = 0.2) and Fourier transformed. Distance constraints were obtained from cross-peak intensities of ROESY experiments, as determined with the XEASY package (*43*). Preliminary structure calculations were performed with the aid of the program DYANA (*44*).

For titration experiments, chemical shift variations of some peptide protons were analyzed as a function of procyanidin B3 concentration using the equation previously described by Charlton et al. (*29*) for a multisite model:

$$\Delta\delta_i = 0.5\Delta\delta_{max}(1 + K_d/n[P_i] + [T_i]/n[P_i]) - \{(1 + K_d/n[P_i] + [T_i]/n[P_i])^2 - 4[T_i]/n[P_i]\}^{1/2} \quad (1)$$

where $\Delta\delta_i$ = change in chemical shift (ppm), $\Delta\delta_{max}$ = maximum change in chemical shift (ppm), K_d = dissociation constant (M), $[P_i]$ = total concentration of peptide (M), n = number of polyphenol binding sites, and $[T_i]$ = total concentration of polyphenol able to fix the peptide. The $[T_i]$ concentration is measured using the relationships described by Charlton and Baxter (*29*, *45*). Calculations were performed using the Microsoft Excel software. For the curve fitting using eq 1, K_d, $\Delta\delta_{max}$, and n were set as adjustable parameters.

Molecular Mechanics. (A) Peptide Alone. Molecular modeling calculations were performed on a SGI Octane R10K workstation running MacroModel (*46*) version 6.5 (Schrödinger Inc.). Conformational minima were found using the modified AMBER* (1991 parameters) force field as implemented and completed in the MacroModel program. Built structures were minimized to a final RMSD gradient ≤ 0.005 kJ·Å^{-1}·mol^{-1} via the truncated Newton conjugate gradient (TNCG) method (1000 cycles). Calculations were performed with the GB/SA continuum solvation model (*47*). The solvent chosen was water. In all cases the extended cutoff option was used throughout (VdW = 8 Å, electrostatic = 20 Å, and H-bond = 4 Å). It must be mentioned that tannins are very simple molecules from a chemical point of view, and hence the corresponding parameters in actual force fields are well-defined and of high quality. This provides accurate 3D models (*48*−*50*).

Stochastic dynamic simulations were accomplished using the variant of molecular dynamics that is implemented in MacroModel. The forces from the force field were augmented by frictional and random forces that simulate some properties of a solvent medium (*63*). The chosen temperatures were 300, 500, and 1000 K, the time step was 1.5 fs for T = 300 K and 1 fs in the other cases, the total simulation time in each case was 2 ns, and 200 snapshots were saved for each run. All saved conformers were fully minimized and ranked by ascending energy (TNCG, 1000 steps).

Minimization and molecular dynamics runs were performed under constraints coming from ROESY experiments. The following distance constraints were chosen according to the NOE correlation intensities: strong, 2.2 ± 0.4 Å; medium, 3.5 ± 0.9 Å; and weak, 5.0 ± 0.5 Å. These distance constraints are chosen in order to ensure three contiguous classes of distances without overlap but also without any "forbidden" intervals.

(B) Peptide−Tannin Systems. Calculations were performed with and without the intermolecular NMR constraints but always starting from the previously found peptide conformation, determined using intramolecular NMR constraints.

For calculations performed with intermolecular NMR constraints, the B3 molecule previously built with calculated NMR coupling constants corresponding to the experimental data was used throughout (*36*) (results to be published elsewhere). Because there are very few modifications in NOE and J values upon tannin addition, the lowest energy conformer of peptide $IB7_{14}$ found at 1000 K was used. The intermolecular NOE constraints were added, and the calculation ran for 2 ns.

Calculations were also performed by removing the intermolecular NMR constraints. In this case, after full minimization, two systems were studied with different $IB7_{14}$/B3 molar ratios: system A with a 1/1 ratio and system B with a 1/4 ratio. GB/SA continuum solvation was systematically used with water as solvent and with the extended cutoff option. Five different 2 ns runs were performed with system A and two different 5 ns runs with system B, with tannins randomly positioned around the peptide. In each case a snapshot was stored every 10 ps.

Following the constrained molecular dynamics runs, a cluster analysis was performed with XCluster 1.1 (*51*) as implemented within MacroModel. For this purpose, we used a distance criterion selection as the RMS difference between corresponding all heavy atoms in pairs of structures. This approach leads to a set of clusters, each of them being a family of conformers. In Xcluster, a conformer belongs to a cluster if it lies within the threshold distance of any component of this cluster and at more than this threshold distance of all components of all other clusters.

(C) Calculation of Amphiphilic Surfaces. Molecular lipophilicity potentials (MLP) were calculated at the atomic level with an homemade program originating from an idea of Audry et al. (*52*) and using an exponential function (*53*). The fragmental atomic constants used were those of Broto et al. (*54*), and MLP maps were calculated via the MLPP program (*55*).

RESULTS

Our systems were analyzed by physicochemical techniques, CD, NMR, MS, and molecular modeling. Results are presented accordingly. All CD, NMR, and mass spectrometry experiments were performed in water and water−ethanol (88:12) at low pH (3.5) and room temperature.

Circular Dichroism of $IB7_{14}$ and $IB7_{14}$−B3. CD spectra of $IB7_{14}$ in the absence and presence of tannins (1/0, 1/1,1/2, 1/3 molar ratios) are shown in the Figure 2. The CD contribution of B3 was removed by recording independently the spectrum of the tannin alone in solution. All curves superimpose except that for the 1/3 ratio, where a slight deviation is observed. However, it must be mentioned that, in the latter case, the sample was very diluted due to the successive addition of B3 solution. So the spectrum has a poorer signal-to-noise ratio that may explain the slight deviation from the other curves. It appears that the addition of B3 does not markedly modify the peptide folding. All spectra were deconvoluted according to a procedure already reported (*21*), and all showed a combination of 34% of type II helix and 66% of an extended and random coil conformation, within the experimental error.

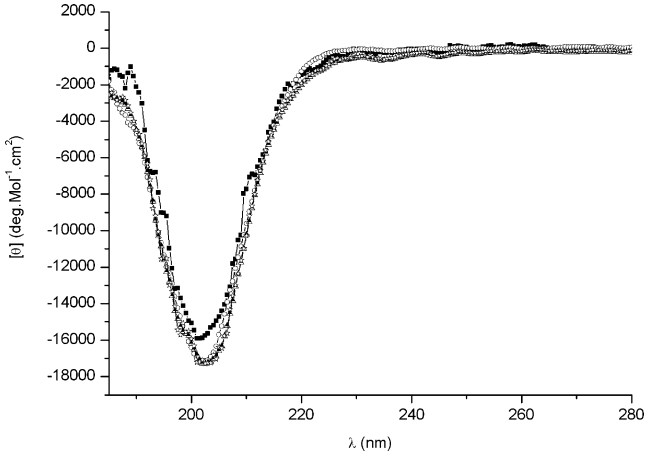

FIGURE 2: Circular dichroism spectra of 200 μM IB7$_{14}$ in the presence and absence of B3 tannin: (open circle) no tannin; (star, triangle, square) 1/1, 1/2, 1/3 peptide/procyanidin B3 molar ratios, respectively. T = room temperature. Spectra are normalized according to the peptide concentration. The procyanidin B3 spectral contribution was removed using data obtained from control experiments with B3 alone in solution.

Nuclear Magnetic Resonance of IB7$_{14}$ and IB7$_{14}$−B3. NMR samples were prepared in water solution. Peptide concentrations ranged from 1 to 5 mM whereas those of B3 varied from 0 to 13 mM. In these conditions, no precipitate could be detected by visual inspection. However, NMR experiments were recorded using the HRMAS technology to take care of the colloidal behavior of these complexes that would otherwise lead to poorly resolved spectra (*56*).

Samples containing the peptide alone were submitted to the classical battery of 2D techniques for structure determination, as described in Materials and Methods. It must be mentioned that DIPSI or HOHAHA were used, without noticeable changes in results. ROESY was used instead of NOESY because of the lack of cross-peak intensities in the latter. No peptide spectral change was observed on the 1−5 mM concentration range. Resonance assignment was performed using the usual procedures, and the chemical shifts, coupling constants, and NOE effects were tabulated (49 NOE and 12 ^3J). This information is available as Supporting Information. The IB7$_{14}$ peptide structure was calculated using the DYANA software and further refined using molecular modeling (vide infra).

Experiments were repeated upon addition of procyanidin B3. NMR parameters were recorded for 10 different peptide/procyanidin B3 molar ratios (1/1 to 1/7 molar ratios). Results are also available as Supporting Information. Several comments can be made. Upon tannin addition, one notices gradual changes in some peptide chemical shifts. They will be discussed in the titration section (vide infra). No supplementary intramolecular NOE was evidenced in the peptide. Very interestingly, intermolecular NOE were detected between the peptide and the procyanidin dimer (Figure 3 and Figure A in Supporting Information). It must be mentioned that no significant variation was observed for the tannin chemical shifts. Among all of the protons of the peptide, four groups of residues appear to be more influenced by an increasing polyphenol concentration: Pro2, Pro6, Pro9-Pro10, and Gly13-Gly14. Figure 4 displays the Pro9-Hα chemical shift variation as a function of the procyanidin/peptide molar ratio. The chemical shift difference values were fitted using eq 1 after the estimation of the procyanidin B3 association constant (K_a) using the method previously described by Baxter et al. (*45*) ($K_a = 1.8\ M^{-1}$). By working with a procedure that allows K_d, n, and $\Delta\delta_{max}$ to vary freely, one finds $K_d = 1.9 \times 10^{-4}$ M, $\Delta\delta_{max} = 0.111$, and $n = 3.2$. The fitting was repeated for peptide protons of Pro2-Hα, Pro2-Hβ, Pro6-Hα, Pro6-Hγ, Pro9-Hα, and Gly13-NH.

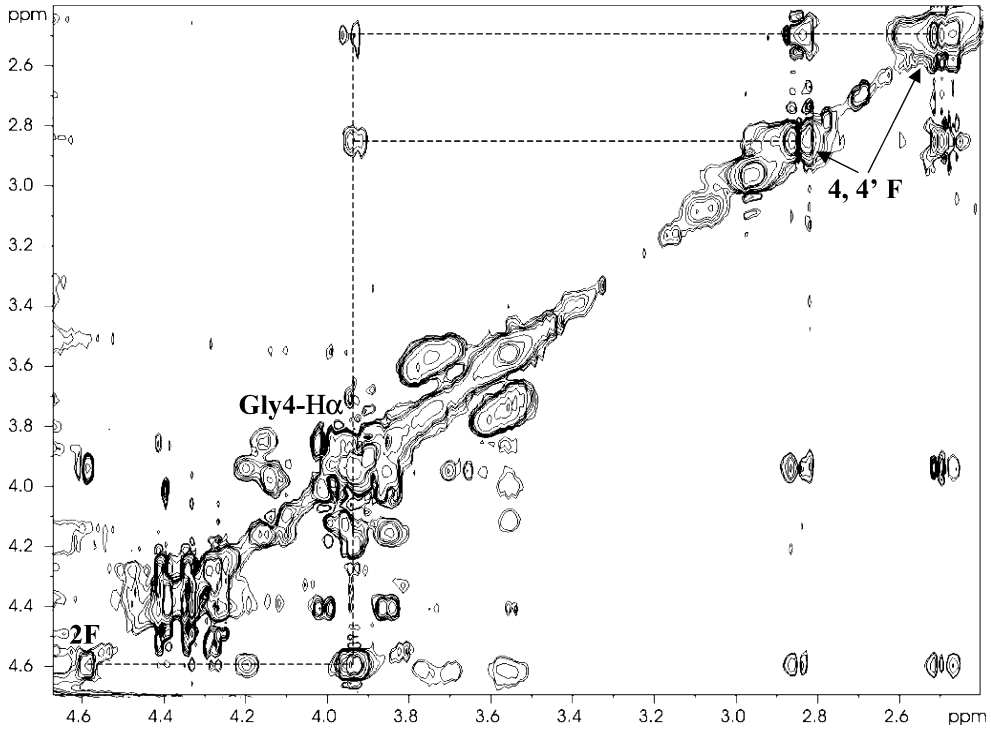

FIGURE 3: Contour plot of the partial ROESY spectrum recorded at 500 MHz, 300 K, and pH 3.5 using a 300 ms spin-lock time of a sample containing 2 mM IB7$_{14}$ and 6 mM B3 (1/3 IB7$_{14}$/B3 molar ratio). Expansion is made in the Hα−Hα region. Only intermolecular NOE effects between Gly4-Hα and 2F, 4F, and 4′F are shown.

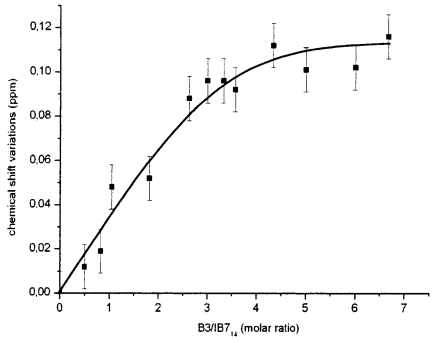

FIGURE 4: Observed (■) and fitted (−) chemical shift differences ($\Delta\delta$) of Pro9-Hα as a function of the B3/IB7$_{14}$ molar ratio. $\Delta\delta$ is calculated with respect to the chemical shift observed in the absence of tannin. Fitting is performed according to eq 1 of the text. Accuracy is 10% (error bars).

Table 1: Thermodynamic Data for the IB7$_{14}$−B3 Complex[a]

residue	K_d (mM)	$\Delta\delta_{max}$	n	χ^2
Pro2-Hα	8.15	0.228	3.0	0.028
Pro2-Hβ	3.00	0.085	3.5	0.015
Pro6-Hα	0.28	0.067	2.6	0.003
Pro9-Hα	0.19	0.111	3.2	0.013
Gly13-NH	2.46	0.186	3.2	0.018

[a] K_d, n, and $\Delta\delta_{max}$ are obtained from NMR chemical shift variations by a least-squares fit of eq 1.

Results are given in Table 1. It is noticed that K_d varies by a factor of 50 around the millimolar value whereas n is about 3. It must be mentioned that the measure of chemical shifts is bound to an intrinsic inaccuracy. Because there is an important overlap of resonances in the regions of interest (particularly for the prolines), one is forced to measure chemical shifts in the 2D maps, which are much less accurate than in 1D spectra. Accuracy then drops down to 0.01 ppm.

Mass Spectrometry of IB7$_{14}$ and IB7$_{14}$−B3. Electrospray ionization, which is known to allow the direct observation of supramolecular assemblies in the gas phase (*57*, *58*), has been used under static sample infusion with nanospray needles. While ensuring low sample consumption, this introduction mode greatly facilitates the recording of CID spectra for complexes having various stoichiometries.

When analyzed alone under nanospray ionization, the isolated IB7$_{14}$ peptide shows a doubly charged ion at m/z 650.9 as the major species (Figure 5A; calculated value 650.83 Th). Premixed peptide−tannin solutions in water−ethanol−acetic acid (89:10:1) were infused in the same way, resulting in the observation in the gas phase of noncovalent IB7$_{14}$−B3 complexes. When infusing a mixture of IB7$_{14}$−B3 premixed at a 1:4 ratio, doubly charged species corresponding to peptide−tannins complexes with 1:1, 1:2, and 1:3 stoichiometries could be isolated in the ion trap, and CID spectra were recorded (Figure 5B−D). A faint signal possibly corresponding to the 1:4 complex was also observed in the full scan mode, but no CID spectrum could be obtained to confirm its identity. The doubly charged species attributed to the 1:1 IB7$_{14}$−B3 complex was observed at m/z 940.0 (calculated value 939.91 Th). Once fragmented in the ion trap, it leads to the doubly charged species of IB7$_{14}$ at m/z 650.9 (Figure 5B). The signal corresponding to the singly charged species of B3 was not observed here, this tannin being less efficiently ionized than IB7$_{14}$ under our source conditions. This 1:1 IB7$_{14}$−B3 complex started to disrupt at 15% collision energy (instrument scale; as an indication, a collision energy higher than 28% is required to fragment the

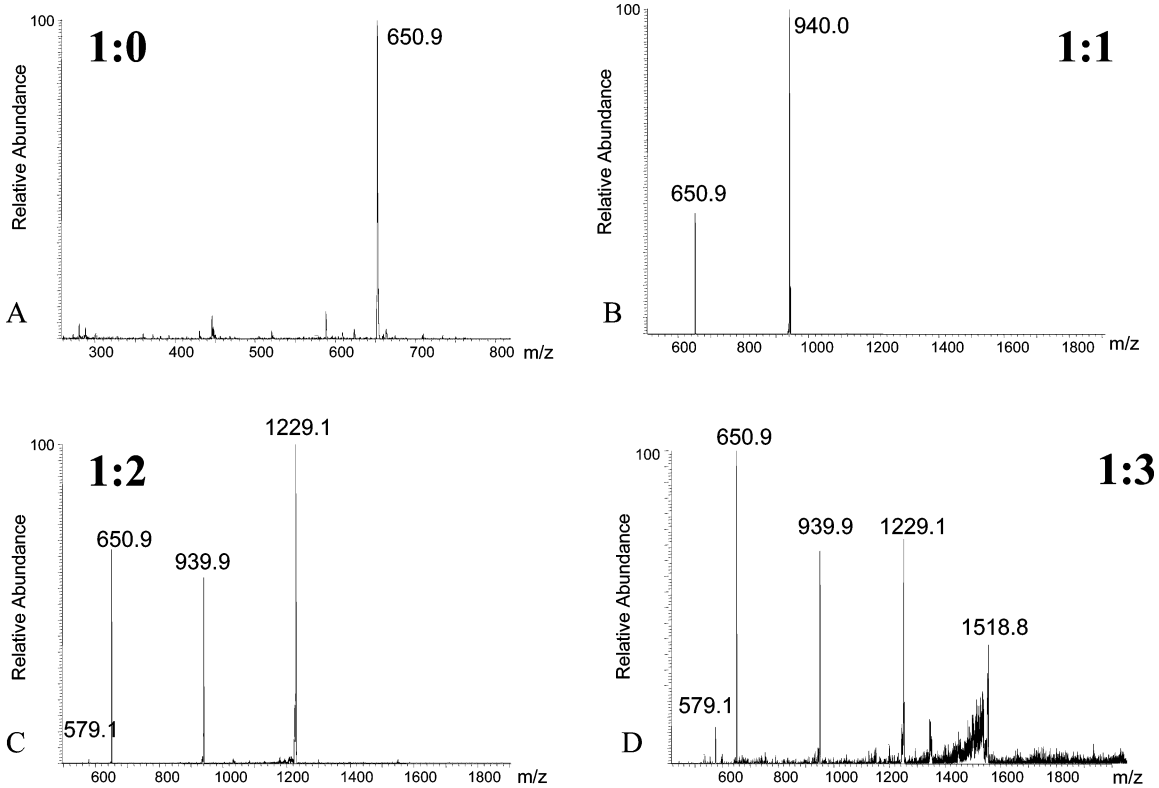

FIGURE 5: ESI mass spectra obtained with a nanospray source for IB7$_{14}$ alone and complexed with one, two, or three procyanidin B3 molecules. Panels: (A) IB7$_{14}$ alone; (B) CID spectrum of a 1:1 IB7$_{14}$:B3 complex; (C) CID spectrum of a 1:2 IB7$_{14}$:B3 complex; (D) CID spectrum of a 1:3 IB7$_{14}$:B3 complex.

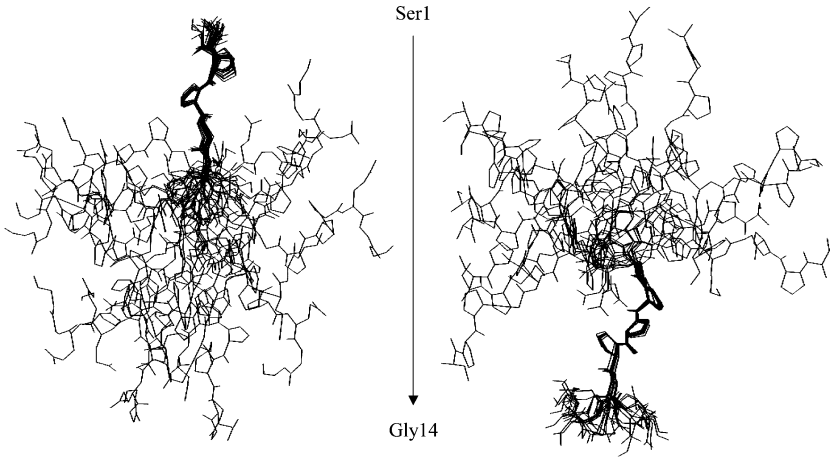

FIGURE 6: Superimposition of the 20 best conformations of $IB7_{14}$ obtained after a molecular dynamic run (2 ns) under NMR constraints. Two independent superimpositions are shown: Pro2 to Pro6 (RMSD = 0.436) (left); Pro9 to Gln12 (RMSD = 0.348) (right).

doubly charged ion of $IB7_{14}$ in the ion trap). At 19% collision energy, the 1:1 complex was almost completely disrupted. As shown on Figure 5C, the 1:2 complex was observed at *m*/*z* 1229.1 (calculated value 1228.98 Th). It splits into a doubly charged species having a 1:1 $IB7_{14}$:B3 stoichiometry, while ions corresponding to $[IB7_{14} + 2H]^{2+}$ and $[B3 + H]^{+}$ are also observed. The behavior of the 1:3 complex under CID conditions is similar, as it splits into 1:2 and 1:1 doubly charged species of these complexes and $[IB7_{14} + 2H]^{2+}$ and $[B3 + H]^{+}$ species (Figure 5D). However, $IB7_{14}$−B3 complexes having 1:1 and 1:2 stoichiometries started to dissociate at energy values of 15% and 18%, respectively (instrument scale), whereas the disruption of the 1:3 complex was only observed above a 22% value.

Molecular Modeling. The peptide structure was calculated from the constraint files obtained by NMR using the DYANA software. The coordinate file was further refined using MacroModel. We performed a continuous long run (2 ns) using stochastic dynamics at various temperatures with continuum solvation (water was used as solvent). In all cases the set of constraints deriving from ROESY measurements was used throughout. Two hundred snapshots were regularly sampled and fully minimized always under constraints. The temperatures chosen were 300, 500, and 1000 K, respectively. As could be expected, the calculation carried out at 300 K proved to be largely inefficient to sample the conformational space during the 2 ns trajectory run. Interestingly, the two experiments conducted at 500 and 1000 K led to almost identical results: the final number of unique conformers is roughly the same (176 and 180, respectively) and the lowest energy conformers were found at −1780.09 kJ·mol^{-1} at 500 K and −1781.84 kJ·mol^{-1} at 1000 K. This indicates that the "melting" at 500 K was sufficient to allow the sampling of the peptide conformational space. The retained solutions are the 20 lowest energy conformers resulting from these two experiments. Figure 6 shows the superimposition of these structures. Superimposition is made by favoring coincidence of residues 2−6 on one hand and residues 9−12 on the other. It can readily be seen that the peptide can be divided into two moieties linked through Gly8, which plays the role of a flexible rotula. These results confirm the extended conformation of the peptide, the type II helix being exclusively represented by the consecutive presence of two (Pro2-Pro3) or three (Pro9-Pro10-Pro11) prolines. The pitch of the type II helix is found to be about 8 Å. The number of residues in the helix of type II is approximately 7, thus giving an amount of secondary structure of 50 ± 10%.

The above procedure was repeated in the case of peptide−tannin complexes. Because there is little variation in the NMR constraints of the peptide in the presence of B3, some of the structures obtained in the absence of B3 were taken together with the B3 structure (*36*), and the five NOE contacts between the Gly4-Hα and Lys5-NH peptide residues and the tannin 2F, 4F, and 4′F protons were added to the list of constraints. We performed a structure calculation of the peptide under constraints with an $IB7_{14}$:B3 molar ratio of 1:1 by the procedure already described. The molecular dynamics run was performed at 500 K and after minimization under constraints; only 40 conformers were retained in an energy range of 100 kJ·mol^{-1}. A cluster analysis was then performed leading to five families. Three of them contained only 1 conformer, and the remaining two contained 11 and 26 conformers, respectively. Figure 7A displays the 26 minimized structures of the principal family superimposed from Pro2 to Pro6. Upon comparison of the superimposition obtained with (Figure 7A) or without B3 (Figure 6), it appears that tannin binding reduces the conformational disorder of the peptide.

Because we have only a few intermolecular constraints from NMR, we decided to perform calculations without these contacts, while keeping intramolecular constraints for both the peptide and the tannin. The first set of calculations was performed by considering a 1:1 complex. The initial peptide structure was taken from the above calculations. The tannin was positioned along the peptide structure starting from residue 1 and going down to residue 14. A minimization step was performed to dock the tannin onto the peptide. It ended up with five different positions along the structure. Five different molecular dynamics calculations were thus performed. At the end of three runs, the B3 molecule was found tightly bound to the peptide. Two sites were evidenced, one in the vicinity of residues Pro2-Pro6 and the other close to Gly8-Pro9, Pro11. In two other runs the B3 dimer was ejected from the peptide contact after 1 ns. Of interest is the finding that one of the sites found by molecular dynamics is also found in the NMR data (vide supra).

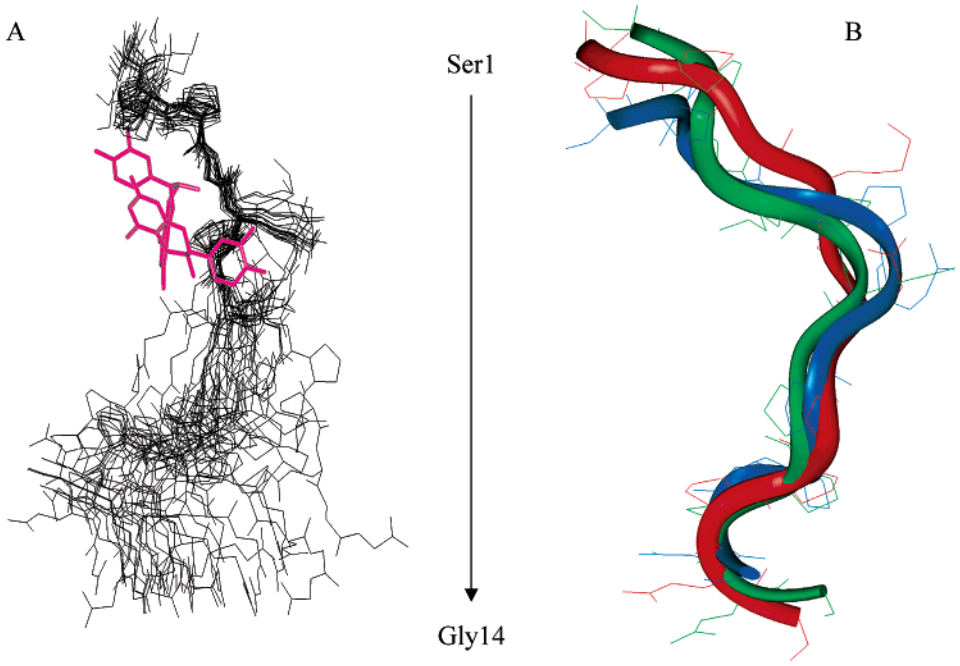

FIGURE 7: (A) Superimposition of the 26 conformations of $IB7_{14}$/B3 (1/1 molar ratio) obtained after cluster analysis (see text). The molecular dynamics were performed during 2 ns under NMR constraints. For purpose of clarity, only one B3 molecule is shown (purple sticks). (B) Superimposition of $IB7_{14}$ backbones (ribbon representation) at the end of molecular dynamics without constraints (blue and green) and with NMR constraints (red). Calculations without constraints were performed in the presence of four tannins (not shown).

Because we found a 1:3 peptide:tannin stoichiometry by mass spectrometry and NMR, we performed calculations by considering that more than three tannins could complex the peptide. Molecular dynamics runs were thus performed by considering a system made of one peptide and four tannin molecules. B3 was positioned at both peptide extremities and oriented at random. Minimization was also performed that ended up with two different starting positions. Two independent molecular dynamic runs were performed for 5 ns. During the two calculations, one of the four B3 dimers was always completely ejected after 2 ns. The last three tannins remained tightly bound to the peptide. The locations were found to be quasi identical for the two runs. One procyanidin is linked to the Pro2 and Pro6 residues, the second one to Pro9 and Pro10, and the third to Gly13 and Gly14 (Figure 8). It is noteworthy that tannins are only found on one face of the peptide. Figure 7B displays the superimposition of the peptide conformations at the end of the two dynamics, together with the peptide conformation obtained under NMR constraints. It is remarkable that all structures superimpose very nicely. One must also indicate that, during the two trajectories, the B3 molecules did not exhibit any noticeable conformational change; i.e., they stayed in the more compact conformation (Figure B in Supporting Information), which is the exclusive conformer present in D_2O (*26*). First, this observation is confirmed by NMR data since no chemical shift change is observed when the peptide:tannin molar ratio increases. Second, two independent molecular dynamics runs were performed during 2 ns in the same conditions as above but on an isolated molecule of B3, starting from two slightly different conformations. They fully confirm that B3 always experienced an identical and very reduced conformational space. As an additional result coming from the calculations, the peptide appears to be stabilized in one conformation probably by hydrogen bonds between the carbonyl of Pro2 and Pro6 and the OH functions of the phenolic part of

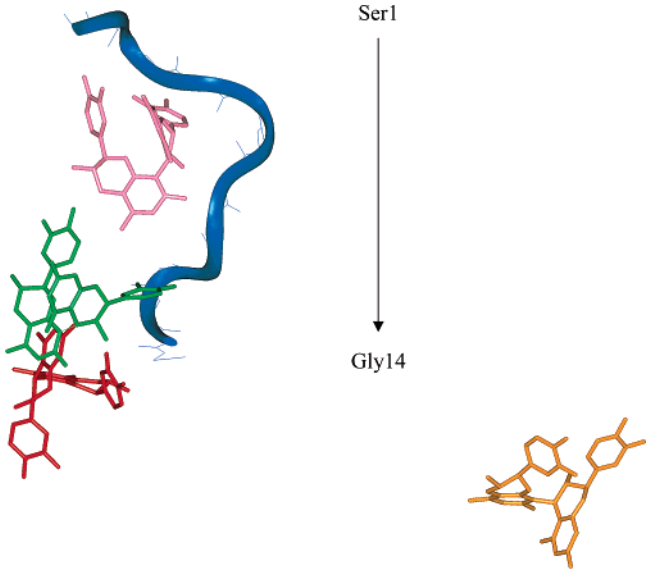

FIGURE 8: Structure of the $IB7_{14}$/B3 (1/4 molar ratio) complex after completion of a 5 ns molecular dynamics run. The protein is shown as a dark blue ribbon with heavy atoms as thin light gray lines. The three bound tannins are shown as purple, green, and red sticks with H-bonds between B3 molecules and protein. The fourth tannin (yellow) was ejected after 2 ns.

procyanidin. The H-bonding pattern is rather complicated, with a majority of H-bonds between the peptide and the catechol phenolic OH but also with the phenolic OH of the benzopyran moiety. It is also worth noting that one H-bond can be found between a carbonyl group of the peptide and the 3-OH of the pyran cycle.

Because tannins appear to bind to only one side of the peptide, we decided to calculate the peptide surfaces that are hydrophilic and lipophilic at the atomic level, as described in Materials and Methods. The starting structure was that coming from the calculation where three tannins are in

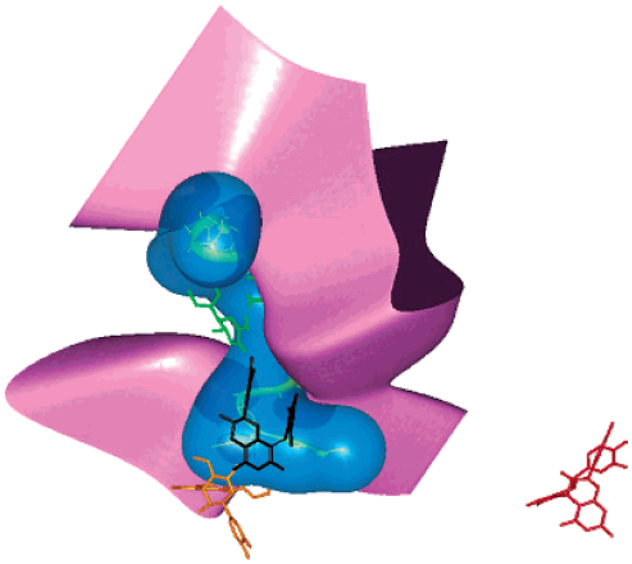

FIGURE 9: Molecular lipophilicity potential contours of $IB7_{14}$. The lowest energy conformation as obtained after a molecular dynamics run ($IB7_{14}$/B3, 1/4) has been used. The trace of the protein is shown as a green ribbon. Hydrophilic potentials are shown as a light blue isosurface whereas the lipophilic counterpart is shown as a red isosurface (not visible in this representation). The purple isosurface represents the interface between lipo- and hydrophilic regions. The four B3 are shown as sticks; the red one in the right lower part has been ejected after 2 ns.

contact with the peptide. As shown in Figure 9 the peptide exhibits an amphiphilic profile: a hydrophilic part shaded in blue and a lipophilic part shaded in red (not visible in the figure). In Figure 9 the boundary between these two regions is shaded in pink. It is remarkable that the peptide structure is separated in two faces of opposite lipophilicity properties. The most lipophilic part of the peptide includes essentially the alkyl chain of Gln7 and Lys5 and γ- and δ-CH_2- of all prolines, the β-CH_2- being always borderline (see Figure C in Supporting Information). It appears that tannins bind to the hydrophilic face that is mainly defined by the peptide backbone (amide, carbonyl, and $-CH_\alpha$ of glycines and prolines).

DISCUSSION

This work reports a new and comprehensive approach for studying, in their natural conditions, the interactions between human salivary peptides and condensed tannins of red wines. Using three experimental techniques and molecular modeling, information on 3D structure, dynamics, stoichiometry and stability of the complex, dissociation constants, and minute description of binding phenomenon could be determined. For the first time, magic angle spinning techniques are used to cope with the colloidal nature of complexes and reach structural resolution. Major results are as follows: (i) The $IB7_{14}$ structure is akin to a helix of type II like polyproline peptides, where glycine 8 seems to play a central role. (ii) Three tannin molecules tightly complex the peptide without modifying its secondary structure, but its conformational disorder appears to be reduced. (iii) Three binding sites are evidenced with a global dissociation constant in the millimolar range. (iv) All tannins bind on the hydrophilic side of the saliva peptide, suggesting that the major interaction forces are governed by hydrogen bonds. All of these points will be developed below and finally discussed in the general frame of wine astringency.

Peptide Structures with and without Tannins. The $IB7_{14}$ peptide displays an extended conformation due to an almost even repartition of type II helix and random coil. The two portions of helix II are separated by the glycine 8 that appears to play the role of a rotula. The helix of type II structure is more opened than a regular α-helix: this is demonstrated by measuring the helix pitch. We found ~8 Å, which is larger than that of the α-helix (5−6 Å). Such type II helices are found in collagens (*59*) and are mainly due to the presence of proline residues. Interestingly, we found almost the same helix II content in the entire IB7 protein (59 aa) (*21*). It has been proposed by Hagerman and Butler (*60*) that this opened and flexible structure is a prerequisite for tannin binding.

Adding procyanidin B3 to $IB7_{14}$ results in the formation of a complex without affecting the secondary structure of the peptide, as demonstrated by CD, NMR, and molecular dynamics. As observed from molecular dynamics calculation, the two helix II parts on both sides of the Gly8 appear to be retained and fixed by three B3 molecules, which results in a loss in degrees of freedom of the peptide. Instead of obtaining a cloud of conformations as depicted in Figure 6, only one of them is favored (Figure 7B). When comparing the results obtained from structure calculation under NMR constraints and molecular dynamics without intermolecular constraints, the two structures coming from the pure calculation nicely superimpose with that obtained using intermolecular constraints. On the other hand, the B3 molecule adopts the more compact form like "tweezers" that offers the maximum of OH group pointing outside, thus favoring H-bonding.

Peptide−Tannin Complexes. There is clear evidence that $IB7_{14}$ and B3 form a 1:3 complex. First, complexes having 1:1, 1:2, and 1:3 stoichiometries have been observed by means of electrospray mass spectrometry. It must be noticed that even if the ionization conditions are quite mild in the MS source, a lot of energy is given to the complexes. The assemblies are stable enough to stand this energy and travel as noncovalently bound species. Furthermore, these complexes were infused at low pH in the presence of ethanol, conditions that most often disrupt noncovalent assemblies involving proteins. Of interest is the fact that one must increase the voltage applied to the ion trap to dissociate the 1:3 complex, in comparison to the value used for the 1:1 or 1:2 complex. This strongly indicates the increased stability of the 1:3 assembly. Second, NMR titration experiments favor a 1:3 association characterized in a noninvasive manner. It is worth mentioning here that we worked at tannin concentrations that were much lower than the B3 self-aggregation constant (1.8 M^{-1}). Fitting of eq 1 indeed leads to a number of binding sites of ca. 3, in all cases. As mentioned in the Results section, K_d values obtained by proton NMR titration bear some inaccuracy, giving us only 1 order of magnitude around the millimolar value. This is nonetheless in accordance with values ranging between 2 and 33 mM as already published for a similar polyphenol (galloyl epigallocatechin) and a 19-mer peptide (*29*). The authors also found a stoichiometry of 3 for their protein−tannin system. Although close to our values, one must mention that the above authors always used 10−20% DMSO to cope with aggregation. In this work HRMAS NMR offers

the advantage of working in a natural medium even in the presence of colloidal particles. At this level of the discussion, it is important to note that the model used to fit our data and those of Charlton (*33*) is not applicable for a cooperative mechanism for B3 fixation (*29*). Our mass spectrometry data suggest that the binding mechanism may be cooperative; hence, our NMR data could be reinterpreted in the light of a new model, when available. Also of interest is the fact that molecular dynamics of a system initially constituted by one peptide and four tannins ends up in a tight 1:3 complex. So we have very strong experimental evidence for a stoichiometry of 1:3 independently of a model.

Detailed Structural Analysis of the Complex. Chemical shift variations of defined peptide protons (Hα of Pro2, Pro6, Pro9, Pro10; NH of Gly13-Gly14) upon B3 addition could be assimilated with interaction sites. This highlights the important role of proline residues for the interaction as already described (*26*, *27*, *29*, *33*, *60*). ROESY experiments performed for a 1:3 molar ratio only led to intermolecular NOE effects between B3 and the Pro2-Pro6 site, thus confirming the existence of this site. When the structure of a 1:1 complex obtained by molecular dynamics using intermolecular NMR constraints is compared to those obtained from calculations in the absence of these constraints, two sites are evidenced: one made by the Pro2 and Pro6 residues and the second by Pro9-Pro10-Pro11. Please note that in this calculation the starting position of B3 was varied from one peptide end to the other. Thus, the positioning of the first site is in complete accordance with the ROESY experiments and the second with the chemical shift variations observed for Pro9-Pro10 protons. The molecular dynamics calculations with a 1:4 molar ratio led to the binding of three tannins, the fourth one being expelled from the complex. Again, there is a complete agreement with the NMR data (ROESY plus chemical shift variations), the third site being identified close to Gly13-Gly14. Since we only detect intermolecular NOE effects between tannin and the Pro2, Pro6 site, it can be suggested that the two other sites are much more dynamic than that detected by ROESY experiments. The contact between tannins and peptide does exist, but the exchange could be interpreted as fast (correlation times shorter than nanoseconds), thus precluding detection of correlations by through-space NMR experiments. Also of interest is the fact that the three binding sites that have been experimentally evidenced by NMR and mass spectrometry are only seen by molecular dynamics when enough tannins are placed around the peptide. For the 1/1 molecular dynamic simulation, only two sites were identified. This could suggest that the binding process may be cooperative, which tells us that the model used to determine K_d (vide supra) is probably not appropriate.

The structure of the complex shows that B3 molecules are fixed always on one side of the peptide; this site has been identified as hydrophilic after our amphiphilicity calculations. This is in agreement with molecular modeling calculations that show the presence of numerous hydrogen bonds between the carbonyl functions of some proline residues and the OH group of the A, D or B, E rings of procyanidins. Conversely, no stacking is observed between the pyrrolidine ring of proline residues and the phenolic rings of procyanidin that would be in favor of a hydrophobic effect. The observation of $IB7_{14}$−B3 complexes using nanospray ionization mass spectrometry also highlights interactions occurring through hydrogen bonds. Indeed, supramolecular complexes involving proteins, while losing hydrophobic interactions, most often survive the desolvation−ionization process in the electrospray source because of the occurrence of hydrogen bonds and electrostatic interactions (*57*, *58*, *61*). It is also interesting to mention that Hagerman and Butler by performing competitive binding assays in water also described proanthocyanidin−protein interactions as being mainly governed by hydrogen bonding (*60*).

The nature of the binding has been widely discussed. Haslam (*27*) described the complexation of polyphenols with proteins as a specific example of molecular recognition, where polyphenols act as multidentate ligands via their aromatic nuclei and phenolic groups, the principal driving force being thought to be the hydrophobic effect. The interaction has been interpreted as an association between the phenol rings and the open, flat, and rigid hydrophobic surface of the pyrrolidine ring of a proline residue (*24*, *26*). These findings appear to be in contradiction with ours. It must, however, be mentioned that their experiments were performed by adding 10−20% DMSO to increase the solubility of their preparations. This may change the hydrophobic/hydrophilic properties of both the tannin and the proteins in this no longer "natural" medium. The delicate balance between the amphiphilic forces may then strongly depend on solvent.

A Molecular Vision of Astringency. Protein−tannin interaction is the source of astringency, the mouth dryness sensation due to the complexation of the lubricant salivary proteins. It is often asked why very different feelings are perceived depending on wines. This may be linked to the specific type of interaction between tannins and proteins that may depend on tannins and protein nature (*30*) and also to the stability and the lifetime of complexes. We have shown herein that the IB7 fragment can complex three B3 tannins and that the interaction occurs in the hydrophilic side of the peptide. The peculiar structure of the peptide can play an important role here. In the absence of tannins it appears very flexible and offers type II helices (proline-rich parts) for binding. Once complexed, the conformational freedom of the peptide, as well as that of the entire complex, appears much reduced. Is this phenomenon related to astringency? It is interesting trying to predict what would be the stoichiometry for B3 interacting with the entire IB7 human saliva protein. Because the $IB7_{14}$ sequence is almost contained three times in IB7, one could guess that a 1/9 complex could be stabilized. If this happened to be true, PRP proteins of the IB7 family could be called "tannin sponges". Whereas the properties of PRP become unveiled, the specificity of the tannin counterpart is more subtle. It probably depends on its chemical nature (hydrolyzable, condensed, galloylated, etc.). Its molecular weight, 3D structure, propensity to autoassociate, and water solubility may lead to noticeable differences in the protein−tannin complex formation. This explains, perhaps, the gustative differences noticed by enologists about tannin behavior in red wine such as drying, puckering, sour, astringent, bitter, or rough character (*62*). Of interest is the fact that the tannin binding sites appear to have different physicochemical properties. In our case the sites appear to have different dynamics. This might be linked to their lifetime that could modulate the time during which

the proteins are complexed and therefore no longer available to lubricate the mouth.

CONCLUSION

The concomitant use of CD, HR-MAS NMR, electrospray ionization mass spectrometry, molecular modeling, and dynamics afforded a comprehensive physicochemical description of PRP−tannin interactions. Information on stoichiometry, affinity constants, binding site localization, nature, and dynamics could be obtained. Of importance, all experiments were accomplished in a medium very close to the natural environment, i.e., the mouth saliva.

ACKNOWLEDGMENT

We thank Philippe Picard (UBS, Bordeaux) for help in debugging GIFA, XEASY, and DYANA programs and Katell Bathany and Marc Bonneu (University Bordeaux 2) for help in mass spectrometric measurements.

SUPPORTING INFORMATION AVAILABLE

Four tables giving proton chemical shifts, ^3J scalar coupling constants, and intra- and intermolecular NOE effects of $IB7_{14}$ and three figures showing a contour plot of partial ROESY spectra, a superimposition of the 4/1 tannin/$IB7_{14}$ system, and molecular lipophilicity potentials. This material is available free of charge via the Internet at http://pubs.acs.org.

REFERENCES

1. Joslyn, M. A., and Goldstein, J. L. (1964) *Astringency of fruit and fruit products in relation to phenolic content* (Mrack, M. E., and Stewart, G. F., Eds.) Academic Press, New York and Chichester.
2. Green, B. G. (1993) *Acta Psychol.*, 84−119.
3. Prinz, J. F., and Lucas, P. W. (2000) *J. Oral Rehabil. 27*, 991−994.
4. Bate-Smith, E. C. (1954) *Food 23*, 124.
5. Kallithraka, S., Bakker, J., and Clifford, M. N. (1998) *J. Sens. Stud. 13*, 29−43.
6. Haslam, E. (1998) *Practical Polyphenolics*, Cambridge University Press, Cambridge, U.K.
7. Gawel, R. (1998) *Aust. J. Grape Wine Res. 4*, 74−95.
8. Ribéreau-Gayon, P. (1972) *Plant phenolics*, Oliver and Boyd, Edinbourg.
9. Bennick, A., McLaughlin, A. C., Grey, A. A., and Madapallimattam, G. (1981) *J. Biol. Chem. 256*, 4741−4746.
10. Kauffman, D. L., and Keller, P. J. (1979) *Arch. Oral Biol. 24*, 249−256.
11. Bennick, A. (1982) *Mol. Cell. Biochem. 45*, 83−99.
12. Beeley, J. A. (2001) *Oral Dis. 7*, 69−70.
13. Gron, P., and Hay, D. I. (1976) *Arch. Oral Biol. 21*, 201−205.
14. Hatton, M. N., Loomis, R. E., Levine, M. J., and Tabak, L. A. (1985) *Biochem. J. 230*, 817−820.
15. Bergey, E. J., Levine, M. J., Reddy, M. S., Bradway, S. D., and Al-Hashimi, I. (1986) *Biochem. J. 234*, 43−48.
16. Mehansho, H., Clements, S., Sheares, B. T., Smith, S., and Carlson, D. M. (1985) *J. Biol. Chem. 260*, 4418−4423.
17. Mehansho, H., Ann, D. K., Butler, L. G., Rogler, J., and Carlson, D. M. (1987) *J. Biol. Chem. 262*, 12344−12350.
18. Lu, Y., and Bennick, A. (1998) *Arch. Oral Biochem. 43*, 717−728.
19. Kauffman, D. L., Keller, P. J., Bennick, A., and Blum, M. (1993) *Crit. Rev. Oral Biol. Med. 4*, 2287−2292.
20. Stubbs, M. J., Chan, J., Kwan, A., So, J., Barcynsky, U., Rasooulit-Rashti, M., Robinson, R., and Bennick, A. (1998) *Arch. Oral Biol. 43*, 753−770.
21. Simon, C., Pianet, I., and Dufourc, E. J. (2002) *J. Pept. Sci. 9*, 125−131.
22. Breslin, P. A. S., Glimore, M. M., Beauchamp, G. K., and Green, B. G. (1993) *Chem. Sens. 18*, 405−417.
23. de Lorgeril, M., Salen, P., Paillard, F., Laporte, F., Boucher, F., and de Leiris, J. (2002) *Cardiovasc. Res. 54*, 503−515.
24. Hatano, T., and Hemingway, R. W. (1996) *J. Chem. Soc., Chem. Commun. 6*, 2537.
25. Vergé, S., Richard, T., Moreau, S., Nurich, A., Merillon, J. M., Vercauteren, J., and Monti, J. P. (2002) *Biochim. Biophys. Acta 1571*, 89−101.
26. Hatano, T., Yoshida, T., and Hemingway, R. W. (1999) in *Plant polyphenol 2: Chemistry, Biology, Pharmacology, Ecology* (Gross, G. G., Hemingway, R. W., and Yoshida, T., Eds.) pp 509−526, Plenum Publishers, New York.
27. Haslam, E. (1996) *J. Nat. Prod. 59*, 205−215.
28. Murray, N. J., Williamson, M. P., Lilley, T. H., and Haslam, E. (1994) *Eur. J. Biochem. 219*, 923−935.
29. Charlton, A. J., Baxter, N. J., Khan, M. L., Moir, A. J. G., Haslam, E., Davies, A. P., and Williamson, M. P. (2002) *J. Agric. Food Chem. 50*, 1593−1601.
30. De Freitas, V., and Mateus, N. (2001) *J. Agric. Food Chem. 49*, 940−945.
31. Charlton, A. J., Baxter, N. J., Lilley, T. H., Haslam, E., McDonald, C. J., and Williamson, M. P. (1996) *FEBS Lett. 382*, 289−292.
32. Sarni-Manchado, P., Cheynier, V., and Moutounet, M. (1999) *J. Agric. Food Chem. 47*, 42−47.
33. Baxter, N. J., Lilley, T. H., Haslam, E., and Williamson, M. P. (1997) *Biochemistry 36*, 5566−5577.
34. Hagerman, A. E., and Butler, L. G. (1980) *J. Agric. Food Chem. 28*, 944−947.
35. Tückmantel, W., Kozinowski, A. P., and Romanczyk, J. (1999) *J. Am. Chem. Soc. 121*, 12073−12081.
36. Barathieu, K. (2002) Thesis, Université Bordeaux 1, Bordeaux.
37. Barathieu, K., Fouquet, E., Dufourc, E. J., Pianet, I., Saucier, C., and Glories, Y. (2002) in *XXIth International Conference on Polyphenols* (Hadrami, I. E., Ed.) pp 551−552, Marrakech, Morocco.
38. Goetz, M., Carlotti, C., Bontemps, F., and Dufourc, E. J. (2001) *Biochemistry 40*, 6534−6540.
39. Piotto, M., Saudek, V., and Sklenar, V. (1992) *J. Biomol. NMR 2*, 661−666.
40. Marion, D., and Wüthrich, K. (1983) *Biochem. Biophys. Res. Commun. 113*, 967−974.
41. Malliavin, T. E., Pons, J. L., and Delsuc, M. A. (1996) *J. Biomol. NMR 8*, 445−452.
42. Malliavin, T. E., Pons, J. L., and Delsuc, M. A. (1998) *Bioinformatics 14*, 624−631.
43. Eccles, C., Güntert, P., Billeter, M., and Wüthrich, K. (1991) *J. Biomol. NMR 1*, 111−130.
44. Günter, P., Mumenthaler, C., and Wüthrich, K. (1997) *J. Mol. Biol. 273*, 283−298.
45. Baxter, N. J., Williamson, M. P., Lilley, T. H., and Haslam, E. (1996) *J. Chem. Soc., Faraday Trans. 92*, 231−234.
46. Mohamadi, F., Richards, N. G. J., Guida, W. C., Liskamp, R., Lipton, M., Caufield, C., Chang, G., Hendrikson, T., and Still, W. C. (1990) *J. Comput. Chem. 11*, 441.
47. Still, W. C., Tempczyk, A., Hawley, R. C., and Hendrikson, T. (1990) *J. Am. Chem. Soc. 112*, 6127.
48. Vivas, N., Glories, Y., Pianet, I., Barbe, B., and Laguerre, M. (1996) *Tetrahedron Lett. 37*, 2015−2018.
49. Saucier, C., Guerra, C., Pianet, I., Laguerre, M., and Glories, Y. (1997) *Phytochemistry 46*, 229−234.
50. Saucier, C., Pianet, I., Laguerre, M., and Glories, Y. (1998) *J. Chim. Phys. 95*, 357−365.
51. Shenkin, P. S., and McDonald, D. Q. (1994) *J. Comput. Chem. 15*, 899−916.
52. Audry, E., Dubost, J. P., Colleter, J. C., and Dallet, P. (1986) *Eur. J. Med. Chem. 21*, 71−72.
53. Fauchère, J. L., Quarendon, P., and Kaetterer, L. (1988) *J. Mol. Graphics 6*, 203−206.
54. Broto, P., Moreau, G., and Vandycke, C. (1984) *Eur. J. Med. Chem. 19*, 71−78.
55. Laguerre, M., Saux, M., Dubost, J. P., and Carpy, A. (1997) *Pharm. Sci. 3*, 217−222.
56. Mirabel, M., Glories, Y., Pianet, I., and Dufourc, E. J. (1999) *J. Chim. Phys. 96*, 1629−1634.

57. Robinson, C. V., Chung, E. W., Kragelhund, B. B., Knudsen, J., Aplin, R. T., Poulsen, F. M., and Dobson, C. M. (1996) *J. Am. Chem. Soc. 118*, 8646−8653.
58. Loo, J. A. (1997) *Mass Spectrom. Rev. 16*, 1−23.
59. Ramachandran, G. N., and Ramakrishnan, C. (1976) in *Biochemistry of collagen* (Ramachandran, G. N., and Reddi, A. H., Eds.) pp 45−84, Plenum Press, New York.
60. Hagerman, A. E., and Butler, L. G. (1981) *J. Biol. Chem. 256*, 4494−4497.
61. Vergé, S., Richard, T., Moreau, S., Richelme-David, S., Vercauteren, J., Promé, J. C., and Monti, J. P. (2002) *Tetrahedron Lett. 43*, 2363−2366.
62. Lee, C. B., and Lawless, H. T. (1991) *Chemical Sens. 16*, 225−238.
63. Van Gunstern, W. F., and Berendsen, M. J. C. (1988) *Mol. Simul. 1*, 173.

BI034354P